Three-dimensional microstructure of samples recovered from asteroid 25143 Itokawa: Comparison with LL5 and LL6 chondrite particles

AUTHOR(S):

Tsuchiyama, Akira; Uesugi, Masayuki; Uesugi, Kentaro; Nakano, Tsukasa; Noguchi, Ryo; Matsumoto, Toru; Matsuno, Junya; ... Abe, Masanao; Yada, Toru; Fujimura, Akio

CITATION:

Tsuchiyama, Akira ...[et al]. Three-dimensional microstructure of samples recovered from asteroid 25143 Itokawa: Comparison with LL5 and LL6 chondrite particles. Meteoritics & Planetary Science 2013, 49(2): 172-187

ISSUE DATE:

2013-08-09

URL:

http://hdl.handle.net/2433/196873

Three-dimensional microstructure of samples recovered from asteroid 25143 Itokawa: comparison with LL5 and LL6 chondrite particles

Akira Tsuchiyama[1]*, Masayuki Uesugi[2], Kentaro Uesugi[3], Tsukasa Nakano[4], Ryo Noguchi[5], Toru Matsumoto[5], Junya Matsuno[1], Takashi Nagano[5], Yuta Imai[5], Akira Shimada[5], Akihisa Takeuchi[3], Yoshio Suzuki[3], Tomoki Nakamura[6], Takaaki Noguchi[7], Masanao Abe[2], Toru Yada[2], Akio Fujimura[2]

[1]Division of Earth and Planetary Sciences, Graduate School of Science, Kyoto University, Kiashirakawa Oiwake-cho, Sakyo-ku, Kyoto 606-8052, Japan.
[2] Japan Aerospace Exploration Agency (JAXA), Institute of Space and Astronautical Science (ISAS), 3-1-1 Yoshinodai, Sagamihara, Kanagawa 229-8510, Japan.
[3] SPring-8, Japan Synchrotron Research Institute (JASRI), 1-1 Koto, Sayo, Hyogo 679-5198, Japan.
[4] Geological Survey of Japan, The National Institute of Advanced Industrial Science and Technology (AIST), 1-1-1 Higashi, Tsukuba, Ibaraki 305-8567, Japan.
[5] Department of Earth and Planetary Sciences, Graduate School of Science, Osaka University, Toyonaka 560-0043, Japan.
[6] Department of Earth and Planetary Material Sciences, Faculty of Science, Tohoku University, Aoba, Sendai, Miyagi 980-8578, Japan.
[7] College of Science, Ibaraki University, 2-1-1 Bunkyo, Mito, Ibaraki 310-8512, Japan.
*Corresponding author E-mail: atsuchi@kueps.kyoto-u.ac.jp

Abstract

In this study, the three-dimensional (3D) microstructure of forty-eight Itokawa regolith particles was examined by synchrotron microtomography at SPring-8 during the preliminary examination of Hayabusa samples. Moreover, the 3D microstructure of particles collected from two LL6 chondrites (Ensisheim and Kilabo meteorites) and an LL5 chondrite (Tuxtuac meteorite) was investigated by the same method for comparison. The modal abundances of minerals, especially olivine, bulk density, porosity, and grain size are similar in all samples, including voids and cracks. These results show that the Itokawa particles, which are surface materials from the S-type asteroid Itokawa, are consistent with the LL chondrite materials in terms of not only elemental and isotopic composition of the minerals but also 3D microstructure. However, we could not determine whether the Itokawa particles are purely LL5, LL6, or a mixture of the two. There was no difference between the particles collected from Rooms A and B of the sample chamber, corresponding to the sampling sequence of the spacecraft's second and first touchdowns, respectively, was detected because of the statistically small amount of particles from Room B.

1. Introduction

Regolith particles were successfully recovered from the S-type asteroid 25143 Itokawa by the Hayabusa mission and received a preliminary examination (PE) (Nakamura et al., 2011; Yurimoto et al., 2011; Ebihara et al., 2011; Noguchi et al., 2011; Tsuchiyama et al., 2011; Nagao et al., 2011; Naraoka et al., 2012; Nakamura et al., 2012). This is not only the first sample recovered from an asteroid and returned to Earth, but also the second extraterrestrial regolith to have been sampled, the first being the Moon, which was sampled by the Apollo and Luna missions (e.g., Heiken et al., 1991). The preliminary examination suggested that the samples are LL chondrite materials (Nakamura et al., 2011; Tsuchiyama et al., 2011; Yurimoto et al., 2011), which suffered space weathering (Noguchi et al., 2011), as indicated by the ground-based telescope observations (Binzel et al., 2001) and remote sensing observations made by the Hayabusa spacecraft (Abe et al., 2006). The textures and compositional heterogeneity of the minerals show that most of the particles (~90%) are similar to LL5 and LL6 chondrites, while the rest of them (~10%) are similar to LL4 chondrites (Nakamura et al., 2011; Tsuchiyama et al., 2011). The particle-shape distribution suggests that the particles are impact fragments on the asteroid surface (Tsuchiyama et al., 2011). The processes prevailing on Itokawa's surface, such as space weathering (Noguchi et al., 2011), solar wind implantation (Nagao et al., 2011), and grain surface erosion (Tsuchiyama et al., 2011; Matsumoto et al. 2012), were revealed.

Forty particles ranging from 30 to 180 μm in size were examined on the basis of the flow chart obtained from the preliminary examination (Nakamura et al., 2011). The total volume of the particles was 4.23×10^6 μm^3, which corresponds to a sphere 201 μm in diameter (Tsuchiyama et al. 2011). However, such a sample size is considerably smaller than the typical textural size of LL chondrites (e.g., typical chondrule diameter is ~570 μm: Nelson and Rubin, 2002). Therefore, it is necessary to exercise caution when comparing the textures of Itokawa particles with those of LL chondrites.

X-ray micro-tomography is a powerful nondestructive method for obtaining the three-dimensional (3D) microtextures and external shapes of samples, especially those with sub-micron spatial resolution. This technique was successfully applied to cometary samples collected during the Stardust mission (Nakamura et al., 2008a,b; Rietmeijer et al., 2008; Tsuchiyama et al., 2009; Iida et al., 2010). In the preliminary examination of the Hayabusa sample, the systematic utilization of this method enabled the effective analysis of the samples (Tsuchiyama et al., 2011, 2012; Nakamura et al., 2011; Yurimoto et al., 2012). However, this technique has not yet been applied to LL chondrites having the same resolution.

The particles examined were collected from Room A of the sample chamber, which corresponds to the sampling sequence at the spacecraft's second touchdown. However, the particles collected from Room B, corresponding to the first touchdown, have not been examined yet. The samples are from the smooth terrain of the MUSES-C Regio

(Yano et al., 2006). The two estimated touchdown locations are different from each other (Yano, private communication), and the regolith at the first touchdown site (particles form Room B) was expected to be affected by space weathering to a greater extent than the regolith at the second touchdown site (particles from Room A), considering the topography near the sampling sites.

In this study, the 3D structures of additional Itokawa particles from Rooms A and B that were newly allocated for PE were examined by x-ray microtomography. In addition to the Itokawa samples, particles from LL5 and LL6 chondrite fragments were also examined by the same method for comparison. This study aims to clarify (1) whether or not Itokawa particles are really LL chondrites in terms of their 3D microtexture and whether it is possible to differentiate between LL5 and LL6 materials, and (2) whether there is any difference between particles from Rooms A and B; finally, PE microtomography results including the modal abundances of minerals, porosities, bulk chemical compositions, and particle-size and particle-shape distributions are reported.

2. Experiments

2-1. Samples

All the Itokawa particles examined by microtomography in the preliminary examination are listed in Table 1. The newly examined samples are four particles from Room A (RA-QD02-0017, 0033, 0049-2 and 0064) and four from Room B (RB-QD04-0006, 0023, 0025 and 0049) (Table 2). These particle samples were obtained from quartz plates by tapping the sample catcher (tapping samples) (Nakamura et al., 2011). Room-A particles were collected from the same area of the above-mentioned quartz plate. The tapping samples from Room B were newly prepared during sample curation at JAXA. Fifteen particles from the Ensisheim meteorite (LL6), ten particles from the Kilabo meteorite (LL6), and fifteen particles from the Tuxtuac meteorite (LL5) were used. Pieces of the meteorites were crushed by gently hitting a larger meteorite piece against the tips of tweezers. Fragmented particles having similar size to the Itokawa particles were randomly collected. Strictly speaking, the crushing of the LL chondrite samples in the laboratory is not the same as that of the Itokawa samples on the asteroid surface by impacts (Tsuchiyama et al., 2011). Therefore, attention is needed when comparing textures related to crushing.

2-2. X-ray microtomography

The sample particles were imaged grain-by-grain by synchrotron radiation (SR) x-ray absorption imaging tomography with a Fresnel zone plate (Uesugi et al., 2006; Takeuchi et al., 2009) at the SPring-8 BL47XU beamline, Hyogo, Japan. The experimental procedure and conditions were essentially the same as those in a previous study (SOM in Tsuchiyama et al., 2011). Each particle was attached to the end of an amorphous carbon fiber of 5 μm in diameter with glycol phthalate, except for the four

particles from Room A for which a glass fiber of 5 μm in diameter was used instead of a the carbon fiber. The CT images were reconstructed from 1800 projection images (0.1 deg/projection) by using a convolution back-projection algorithm (Nakano et al., 2000). It took about 40 min to image one particle. The three-dimensional (3D) structure was obtained by stacking successive CT images taken of different slices through the particle.

The use of x-ray energies of 7 and 8 keV enabled the identification of minerals in the CT images because the K-adsorption edge of Fe at 7.11 keV is present between the two energies (see details of the analytical dual-energy microtomography in Tsuchiyama et al., 2012). The values of linear attenuation coefficients (LACs) in the CT images were obtained by calibrating the LAC values of the standards, which had already been measured at SPring-8 (Tsuchiyama et al., 2005). The chemical composition of olivine, pyroxene, and plagioclase were obtained using the LAC values. A successive set of 3D CT images showing a quantitative 3D mineral distribution was obtained for each particle.

Two different imaging-system settings were used for samples having different sizes: (1) a voxel (pixel in 3D) size of 84–97 nm (effective spatial resolution of ~200 nm) for small samples (≤100 μm), (voxel sizes are 84.0 and 96.2 nm at 7 and 8keV, respectively, for the four Room-A particles and the small particles of the Ensisheim and Kilabo meteorites, while they are 84.2 and 97.1 nm at 7 and 8keV, respectively, for the four Room-B particles and the particles of the Tuxtuac meteorite) and (2) a voxel size of ~250 nm (effective spatial resolution of ~500 nm) for large samples (≥100 μm) (voxel sizes are 228 and 266 nm at 7 and 8keV, respectively, for the large particles of the Ensisheim and Kilabo meteorites).

2-3. Image procedure and analysis

We used the “Slice” software package (Nakano et al., 2006) to process and analyze the 3D CT images. The method is the same as that employed in a previous study (SOM in Tsuchiyama et al. 2011). A solid object was extracted three-dimensionally by binarization of the CT images. The volume of each particle was obtained from the number of voxels on the solid object and the voxel size. The sphere-equivalent diameter was calculated from the volume. The cracks and most of the pores in the small sample particles are three-dimensionally connected outward. These “open pores” were recognized by the wrapping method (Tsuchiyama et al., 2007), and their porosities were eventually obtained. The shape of each solid object was approximated by the best-fit ellipsoid (Ikeda et al. 2000). The longest, middle and shortest axial lengths, *a*, *b* and *c*, respectively, of each object were obtained from the ellipsoid.

The modal abundances of minerals in vol% were obtained from the histograms of the LAC values in the CT images at 7 and 8 KeV by the method used by Tsuchiyama et al. (2011). Although the errors could not be precisely evaluated, the errors for olivine, low- and high-Ca pyroxene, plagioclase, and troilite are low (on the order of 10%)

while those of the minor minerals are relatively large (on the order of 50%) (SOM in Tsuchiyama et al., 2011). The modal abundances in wt% were calculated from the vol% and the densities estimated from the mean chemical composition of the minerals (Nakamura et al., 2011).

3. Results

3-1. Size and shape parameters of Itokawa particles

The results are summarized in Table 1. The total volumes, sphere-equivalent diameters, and median diameters of the samples are shown in Table 2. The total volume of the examined Itokawa samples is similar to that of the LL chondrite samples. However, the volume of Room-B is significantly less than that of Room-A samples (only 0.8 vol% of the total Itokawa sample volume), and the volume of the LL5 chondrite samples is less than that of the LL6 chondrite samples (11.4 vol% of the total LL chondrite sample volume). The median diameter of Room-B samples (24.7 μm) is slightly smaller than that of Room-A samples (36.4 μm), and the median diameter of the LL6 chondrite samples (58.5 μm) is slightly greater than that of the Itokawa samples (33.5 μm).

The cumulative distribution of the sphere-equivalent diameter of all particles (47 particles) including the previous samples (40 particles) is shown in Figure 1. In this data set, the data for particle RA-QD02-0049-2 were excluded because it is the broken piece of an original particle (Ebihara et al., 2011). The log slope of the cumulative distribution is about −2, which did not differ from previous estimates (Tsuchiyama et al., 2011). The sizes of 164 particles, which were collected from the tapping samples in Rooms A and B for the 1st International Announcement of Opportunity for HAYABUSA Sample Investigation by JAXA (http://hayabusaao.isas.jaxa.jp/), were also measured by a scanning electron microscope (SEM). The log slope of their cumulative distribution is also about −2 (Fig. 1). This confirms that the slope corresponding to the fine particles (5 to 100 μm) on the smooth terrain is around −2.

The shape distribution of the present samples, except for RA-QD02-0049-2 (47 particles) (Fig. 2), is almost the same as those of the previous 40 particles. The mean b/a and c/a values are 0.72 ± 0.13 and 0.44 ± 0.15, respectively, (b/a = 0.72 ± 0.13 and c/a = 0.43 ± 0.14: Tsuchiyama et al., 2011) and are similar to the mean axial ratio of fragments generated in laboratory impact experiments (a:b:c ≈ 2:$\sqrt{}$2:1 or b/a ≈ 0.71 and c/a ≈ 0.5: Fujiwara et al., 1978; Capaccioni et al., 1984). The distributions of polymineralic and monomineralic particles are not significantly different, as indicated by the Kolmogorov−Smirnov (K−S) test (probability, P = 0.48), because the monomineralic particles are polycrystalline and are not affected by anisotropic properties, such as cleavage (Tsuchiyama et al., 2011). The K−S test indicates that the shape distribution of the Itokawa particles is not significantly different from that of the laboratory experimental fragments of Capaccioni et al. (1984) (P = 0.22).

3-2. Modal abundances of minerals

The modal abundances of the minerals are shown in Table 3. The modal abundances for the 48 Itokawa particles agree well with those for the 40 particles sampled by Tsuchiyama et al. (2011) and the LL chondrites sampled by Hutchison (2004) and Dunn et al. (2010), both of which are used as reference. It should be noted that the data of Dunn et al. (2010) are obtained in wt% and are compared with those of the Itokawa samples in wt% in Table 3. The modal abundances of minerals in the LL chondrite particles agree well with those in the Itokawa particles and the reference LL chondrites, especially for olivine, although the abundances of other minerals deviate slightly.

The samples with small volumes show large deviations in their modal mineralogy. The abundances of olivine and Ca phosphates in Room-B particles are larger than those in Room-A particles, and the abundances of plagioclase and troilite in Room-B particles are less than those in Room-A particles. The abundances of olivine, high-Ca pyroxene, plagioclase, and chromite in the LL5 chondrite particles are less than those in the LL6 chondrite particles, and the abundances of low-Ca pyroxene, troilite, and kamacite in the LL5 chondrite particles are greater than those in the LL6 chondrite particles.

The total mass of the Itokawa samples was estimated to be 15.0 μg (14.5 μg: Tsuchiyama et al., 2011) from the modal abundances and densities of minerals, which were calculated from the mean chemical composition of the minerals (Nakamura et al., 2011) (Table 2). Thus, the bulk density is 3.4 g/cm^3. This value is the same as that obtained by a previous study (Tsuchiyama et al., 2011). The bulk chemical composition was also calculated from the abundances of the minerals and their chemical compositions by Nakamura et al. (2013). The total mass and bulk density of the LL chondrite particles are 16.7 μg and 3.4 g/cm^3, respectively.

3.3 Three-dimensional micro-textures

The microtextures of the LL5 and LL6 chondrite particles are similar to those in the Itokawa particles with respect to mineral grains, voids, and cracks (Fig. 3).

(1) Monomineralic and polymineralic textures

Some particles are almost monomineralic (>80 vol.%). The mineral is mostly olivine (Figs. 3A and 3B) but sometimes low-Ca pyroxene or plagioclase. Tiny inclusions of Fe-bearing minerals such as troilite are generally present, even if a particle is nearly 100% monomineralic. Polymineralic particles mainly consist of olivine, low-Ca pyroxene, high-Ca pyroxene, plagioclase, and troilite (Figs. 3C and 3D) having equigranular textures and show annealing by thermal metamorphism. However, some (~10%) of the Itokawa particles show poorly equilibrated textures such as mesostasis (Fig. 1D in Tsuchiyama et al., 2011 and Fig. 3B in Nakamura et al., 2011) and chemical heterogeneities (Fig. 3A in Nakamura et al., 2011). The eight newly examined Itokawa

particles have highly equilibrated textures.

Monomineralic particles should come from the coarse parts of LL5 or LL6 chondrites, which were originally phenocrysts of chondrules or large mineral fragments, while polymineralic particles should come from the fine parts, which were the mesostasis of chondrules or chondrite matrices originally. Note that attenuation x-ray tomography does not detect crystallographic orientation, and thus, grain boundaries in a single mineral cannot be imaged. Therefore, the size of a monomineralic particle is the lower limit of the crystal grain size if it is monocrystalline, while the grain size may be smaller if it is polycrystalline. Grain sizes of a polymineralic particle show similar behavior.

The ratio between monomineralic and polymineralic particles is a rough indicator of mineral grain size in the samples. The numbers and proportions (vol%) of the polymineralic particles are shown in Table 4. Approximately 50 vol% is polymineralic, and thus the rest monomineralic, both in the Itokawa and LL chondrite samples, except for Room-B and LL5 particles.

(2) Voids

Voids are present in the Itokawa and LL chondrite particles. Some particles have relatively large (≥10 μm) and irregular voids, which typically extend outward (Figs. 3E and 3F). Such particles are called “porous.” Porous particles are polymineralic or polycrystalline, even if they are monomineralic. They are apparently formed by volatilization during shock events. However, shock textures such as high dislocation density were not observed (Noguchi et al., 2013). No glass or devitrification products were observed. Such textures might be formed by annealing because of thermal metamorphism of originally porous aggregates of fine materials such as matrix or fine regolith breccia.

Some particles have a large number of relatively small void inclusions (less than a few μm) (Figs. 3G and 3H). They are sometimes accompanied by tiny minerals (Fig. 3B). Many of them are platy and have facets (negative crystals), which are also recognized on the particle surfaces by FE-SEM (field-emission scanning electron microscopy) (Matsumoto et al., 2012). The void platelets define 3D planes (Figs. 4A and 4B). The platelets are parallel to the planes, and the directions of their longest axes are common (Fig. 4C). These planes are present in single crystals, which were recognized by electron backscatter diffraction (EBSD) analysis (Zolensky, a personal communication). The morphology and distribution of small void inclusions strongly suggest that the planes defined by the small inclusions are healed cracks, which were originally formed by a shock event, and negative crystals formed by annealing of cracks.

Some voids are elongated. Their lengths are 10 μm or longer and the diameters are close to those of the small void inclusions. Such voids are called “tubes.” Tubes are sometimes curved (Fig. 3E) or connected with each other to form a Wiener-sausage-like

structure (Fig. 3G). Tubes are not located on planes defined by the small void inclusions (arrows in Fig. 4B). The formation mechanism of void tubes is still controversial.

Void-rich particles account for ~21 and ~6 vol% of the Itokawa and LL chondrite samples, respectively (Table 4). All of them are rich in small void inclusions. Some of them are porous (~9 and 4 vol% in the Itokawa and LL particles, respectively) and have void tubes (~16 vol% in the Itokawa and 2 vol% in the LL particles). Room-B particles are void-rich. Not all LL6 chondrite particles are void-rich, while ~2/3 of the LL5 chondrite particles are void-rich (porous, rich in small void inclusion, or have void tubes).

(3) Cracks

The particles typically contain cracks. Some particles have abundant cracks (~0.1 cracks/μm^2) (Figs. 3I and 3J). The proportion of crack-rich particles in the Itokawa samples (~5 vol%) is smaller than that in the LL chondrite samples (~50 vol%) (Table 4). Room-B samples have no crack-rich particles, while the LL5 chondrite samples have abundant crack-rich particles (~75 vol%). Among the LL6 chondrite samples, the Kilabo meteorite samples are richer in cracks than the Ensisheim meteorite samples.

Cracks in the Itokawa samples could be formed by shock events. High densities of cracks were observed in the olivine particles that were collected from the ductilely deformed region of a run product of laser-induced shock experiments with a maximum shock pressure of 38 GPa (Matsumoto et al., 2012).

(4) Porosity

The porosities obtained from microtomography, which correspond to the microporosities in ordinary chondrites, are caused not only by voids but also by cracks (Tsuchiyama et al., 2011). The Itokawa and LL chondrite samples have porosities ranging from ~0 to 10% (Fig. 5) with an average of 1.5 and 1.9%, respectively (Table 3). These samples show similar porosity abundance frequencies with a sharp peak at <1% and weak and broad peaks at ~4%.

3-4. Particle surface edges: sharp vs rounded

Particles with rounded edges are present only in the Itokawa samples (Fig. 4C in Tsuchiyama et al., 2011). Rounded edges were observed both in monomineralic (Fig. 1C in Tsuchiyama et al., 2011) and polymineralic (Fig. 3E) particles. The presence of rounded edges was confirmed by FE-SEM observations of the surface microstructures (Matsumoto et al., 2012). The rounded surfaces were probably aged by sputtering by solar wind particles (Noguchi et al., 2011) or mechanical abrasion (Tsuchiyama et al., 2011), as proposed by Matsumoto et al. (2012). The 3D shapes of particles with rounded edges are more spherical than those of particles with angular edges (Fig. 2). The proportion of Room-A particles with rounded edges (~35 vol%) is larger than that of Room-B particles (~17 vol%) (Table 4).

4. Discussion

4-1. Size and shape features of Itokawa particles

The particle-size and particle-shape distributions of the Itokawa samples in the present study (Figs. 1 and 2) are essentially similar to those in a previous study (Tsuchiyama et al., 2011). The log slope of the size distribution is around –2 and is shallower than that of the Itokawa boulders (around –3: Saito et al., 2006; Miyamoto et al., 2007; Michikami et al., 2008), indicating the lower abundance of ~10 to 100 μm particles on the smooth terrain of Itokawa (MUSES-C Regio), as proposed with reference to the close-up images of the terrain (Yano et al., 2006). As shown in Figure 1, small depressions are present in the cumulative size distributions of the two types of tapping samples determined by microtomography and SEM at ~40 and ~60 μm, respectively. Because the sizes determined by microtomography are the sphere-equivalent diameters and the longest sizes are identified from the SEM images, both depression locations are real and similar. The depressions could reflect (1) the actual size distribution of the regolith particles on the smooth terrain, (2) an artifact introduced by impact of the spacecraft's sampler horn during sampling, (3) electrostatic levitation of charged particles, (4) levitation due to the thruster jets from the ascending spacecraft, and (5) an artifact produced while tapping during sample collection at the curation facility.

The cumulative size distribution of small 898 particles, which adhere on larger Itokawa particles, was also reported (Nakamura et al., 2012). The log slope is –2.3 in the range of 0.6 to 3 μm and is consistent with the present data. However, we cannot evaluate the meaning of this slope because we do not know whether these secondary particles were actually present on Itokawa's surface or whether they were created or modified during sample collection and curation.

The shape distribution, which cannot be statistically distinguished from that of the laboratory experimental fragments (Capaccioni et al., 1984) (Fig. 2), shows that Itokawa particles are consistent with the results of mechanical disaggregation, primarily as a response to impacts, as discussed by Tsuchiyama et al. (2011).

4-2. Comparison between Itokawa particles and LL chondrite materials.

The modal abundances of minerals in the Itokawa samples, especially olivine, are close to those in the LL chondrite samples and agree with the LL chondrite reference data (Table 3). The bulk density, porosity (Fig. 3), and the porosity frequency pattern (Fig. 5) are also similar in both samples. The 3D microstructures including voids and cracks are common among the Itokawa particles (except for poorly equilibrated samples), and the LL5 and LL6 chondrite particles (Fig. 3). These results show that Itokawa particles are similar to LL chondrite materials in terms of not only the elemental compositions (Nakamura et al., 2011) and oxygen isotopic compositions (Yurimoto et al., 2011) of minerals but also on their 3D microstructure.

(1) How representative of Itokawa are the samples

Nagano et al. (2012) statistically examined errors of the modal abundances of minerals from a small number of samples with heterogeneous textures. If forty particles 32 μm in size from an LL6 chondrite sample are randomly collected, which is comparable to the number and size of the examined Itokawa particles, the error in the abundance of olivine, which is the most abundant mineral, is relatively small (52.4 ± 4.6 vol% in the LL6 chondrite sample) and can be used for comparison with the Itokawa particles, where the relative error in the olivine abundance is ~10% (SOM in Tsuchiyama et al., 2011). In contrast, the abundances of other minerals such as Ca-poor and Ca–rich pyroxenes, plagioclase, and troilite cannot be compared because of their relatively large errors (18.6 ± 3.7, 8.5 ± 2.4, 10.5 ± 2.1, and 7.9 ± 2.8 vol%, respectively, in the LL chondrite sample). In fact, olivine abundances in all Itokawa and LL5 and LL6 samples, as well as the average LL chondrites are similar, although the abundances of other minerals are not (Table 3). In addition, olivine abundances in Ensisheim and Kilabo meteorite samples, in which the volumes and numbers of particles are half those in the Itokawa sample, are also similar. Although olivine abundances in Room-B and LL5 chondrite samples appear to be different from the values corresponding to the LL6 chondrite samples, the measured volume is too small for this difference to be statistically significant. The modal abundances of minerals in the adhered objects on Itokawa particles are different from the LL chondrite values (e.g., olivine abundance is only ~30 vol%) (Nakamura et al., 2012). However, the sample volume (~750 μm^3) is statistically too small (only ~1/6000 of the Itokawa samples) for the comparison even though the number of particles is large (914 particles).

The bulk density of the Itokawa samples (3.4 g/cm^3) is equal to that of the LL chondrite samples (3.4 g/cm^3). However, it seems to be higher than the average bulk density of the LL chondrites measured in hand-specimen meteorites (3.22 ± 0.22 g/cm^3 in Consolmagno et al., 2008; 3.18 ± 0.02 g/cm^3 in Macke, 2010) and lower than the average grain density (3.54 ± 0.13 g/cm^3 in Consolmagno et al., 2008; 3.52 ± 0.01 g/cm^3 in Macke, 2010). The average porosity of the Itokawa samples (1.5%) is close to that of the LL chondrite samples (1.9% on average) but less than the average porosity of the LL chondrites from hand-specimen size samples (8.2 ± 5.5% in Consolmagno et al., 2008; 9.5 ± 0.6% in Macke, 2010). It is reasonable to expect that the porosity of the particles should be lower than that of the hand-specimen meteorites, and thus, the bulk density of the particles should be higher because much of the porosity of the hand specimens will be at a scale larger than the particles measured here.

The proportions of polymineralic particles (Table 4) show a trend similar to the modal abundances of minerals. The proportions in all Itokawa samples, Ensisheim and Kilabo meteorite samples, and the LL5 samples are similar. Therefore, in terms of modal abundances of minerals, bulk density, porosity, and mineral grain size, not only the Itokawa particles examined here (~4 × 10^6 μm^3 in total volume) but also the

particles having the volume close to that of the Ensisheim or Kilabo meteorite samples (~2 × 10^6 μm^3) should be representative of LL chondrite material.

In contrast, the proportions of void-rich and crack-rich particles in all the LL5 and LL6 samples are different from those in the Itokawa particles (Table 4). The higher abundances of crack-rich particles in the chondrites samples than those in the Itokawa particles might be due to the formation of cracks during the crushing of the chondrite samples. The examined Itokawa samples (~4 × 10^6 μm^3 in volume) are not representative of LL chondrite materials in terms of the void microstructure.

(2) Difference between Room-A and Room–B samples

The proportion of particles with rounded edges in Room-B samples is lower than that in Room-A samples. This is inconsistent with the expectation that Room-B particles should be more weathered when compared with Room-A particles. Room-A and Room-B samples are different in terms of other features (olivine abundance, proportion of polymineralic, void-rich, and crack-rich particles). However, these differences should be within the permissible statistical error range because of the small amount of Room-B samples. Therefore, we cannot find any difference between Room-A and Room–B particles. When we consider the comparison between the Itokawa and LL chondrite samples, we require at least the volume of the analyzed Ensisheim or Kilabo meteorite samples, and this roughly corresponds to more than ~20 Room-B particles.

(3) LL5 or LL6 chondrite?

The proportion of polymineralic particles in the LL6 chondrite samples is close to that in the Itokawa samples but is less than that in the LL5 chondrite samples. The difference between the LL6 and LL5 chondrite samples is consistent with the smaller mineral grain size in the LL5 chondrite samples when compared with the LL6 chondrite samples. However, the amount of LL5 chondrite samples may not be enough for good statistics, and thus, we could not determine whether the Itokawa samples correspond to LL5 or LL6 chondrite materials (or a mixture of LL5 and LL6 chondrites) from the microstructure.

5. Summary

In this study, the 3D microstructure of forty-eight Itokawa regolith particles (total volume: ~4.2 x 10^6 μm^3, total mass: ~15.0 μg) was examined by synchrotron radiation microtomography in order to retrieve the modal abundances of minerals, particle size and shape, abundance and shape of pores, abundance of cracks, and roundness of the edges on the particle surface (Table 1). Because the 3D microstructure of LL chondrites has not been examined to date, particles collected from LL6 chondrites (Ensisheim and Kilabo meteorites) and an LL5 chondrite (Tuxtuac meteorite) were also investigated by the same method using the same spatial resolution and compared with the Itokawa particles (Tables 2–4).

The shape distribution of the Itokawa particles (Fig. 2) is consistent with the results

of mechanical disaggregation, primarily as a response to impacts (Tsuchiyama et al., 2011). The cumulative size distribution of the Itokawa particles including the 164 particles measured during the curatorial work at JAXA (Fig. 1) confirms that the log slope for the fine particles (~5 to 100 μm) on the smooth terrain is around –2, which indicates lower abundance of the fine particles on the smooth terrain of Itokawa (MUSES-C Regio) (Tsuchiyama et al., 2011). The modal abundances of minerals in the Itokawa particles (Table 3) are consistent with those in the LL chondrites, which were randomly collected by the spacecraft and at the curation facility (Nagano et al., 2012). The voids in the Itokawa samples are classified into three types: relatively large voids in porous particles, relatively small voids (negative crystals as products of crack healing) and tube-shaped voids. Some of them should be formed by thermal annealing after impact events, which must have occurred on the parental body of Itokawa (Nakamura et al., 2011).

The comparison between the Itokawa and LL chondrite particles results in the following conclusions: (1) The common 3D microstructure including the voids and cracks (Figs. 3 and 5) show that the Itokawa particles are consistent with the LL chondrite materials in terms of not only the modal abundance and elemental (Nakamura et al., 2011) and isotopic composition (Yurimoto et al., 2011) of minerals but also their 3D microstructures. The results definitely confirm that the surface materials on the S-type asteroid Itokawa correspond to LL chondrites, which enable direct validation of the relation between asteroids and meteorites. However, we cannot distinguish the thermally equilibrated Itokawa particles from the LL5 and LL6 chondrites, even with the present resolution. (2) The examined Itokawa particles are representative of LL chondrite materials in terms of modal abundances of minerals, especially olivine, bulk density, porosity, and mineral grain size but not in terms of void microstructures. (3) No difference was detected between the first- and second-touchdown particles (Room-B and Room–A samples, respectively) because of the statistically insufficient number of first-touchdown particles. In addition, Nakamura et al. (2013) reported that the major element composition of the minerals in the first- and second-touchdown particles could not be distinguished. It is important to clarify whether there is any difference between them because the source areas of regolith particles for the two different touchdown sites (~100 m apart: Yano, private communication) may have different space weathering histories. More than 20 Room-B Itokawa particles are required for the comparison.

Acknowledgements

We thank the Hayabusa sample curation team and the Hayabusa project team. We also thank Dr. M. Zolensky of NASA Johnson Space Center for providing the EBSD data of the Itokawa particles. We are grateful to Dr. A. Gucsik of Kyoto University and Max Planck Institute for Chemistry, Mainz, Germany for reading the manuscript. A.

Tsuchiyama was supported by a Grant-in-aid of the Japan Ministry of Education, Culture, Sports, Science and Technology (19104012). The tomography experiment was performed under the approval of the SPring-8 Proposal Review Committee (2010B1531).

References

Abe M., Takagi Y., Kitazato K., Abe S., Hiroi T., Vilas F., Clark B. E., Abell P. A., Lederer S. M., Jarvis K. S., Nimura T., Ueda Y. and Fujiwara A. 2006. Near-infrared spectral results of asteroid Itokawa from the Hayabusa spacecraft. *Science*. 312:1334-1338.

Binzel R. P., Rivikin A., Bus S., Sunshine J. and Burbine T. 2001. MUSES-C target asteroid (25143) 1998 SF36: A reddened ordinary chondrite. *Meteoritics & Planetary Science*. 36:1167-1172.

Capaccioni F., Cerroni P., Coradini M., Farinella P., Flamini E., Martelli G., Paolicchi P., Smithh P. N. and Zappala V. 1984. Shapes of asteroids compared with fragments from hypervelocity impact experiments. *Nature*. 308:832-834.

Consolmagno G. J., Britt D. T., and Macke R. J. 2008. The significance of meteorite density and porosity. *Chemie der Erde - Geochemistry*. 68: 1-29.

Dunn T. L., Cressey G., McSween H. Y. Jr., and McCoy T. J. 2010. Analysis of ordinary chondrites using powder X-ray diffraction: 1. Modal mineral abundances. *Meteoritics & Planetary Science.* 45: 123-134.

Ebihara M., Sekimoto S., Shirai N., Hamajima Y., Yamamoto M., Kumagai K., Oura Y., Ireland T. R., Kitajima F., Nagao K., Nakamura T., Naraoka H., Noguchi T., Okazaki R., Tsuchiyama A., Uesugi M., Yurimoto H., Zolensky M. E., Abe M., Fujimura A., Mukai T. and Yada T. 2011. Neutron activation analysis of a particle returned from asteroid Itokawa. *Science*. 333: 1119-1121.

Fujiwara A., Kamimoto G. and Tsukamoto A., Expected shape distribution of asteroids obtained from laboratory impact experiments. *Nature*. 272:602-603.

Heiken G. H., Vaniman D. T. and French B. M.. eds. 1991. *Lunar Sourcebook: A User's Guide to the Moon.* 756 pp. Cambridge University Press, Cambridge.

Iida Y., Tsuchiyama A., Kadono T., Sakamoto K., Nakamura T., Uesugi K., Nakano T., and Zolensky M. E. 2010. Three-dimensional shapes and Fe contents of Stardust impact tracks: a track formation model and estimation of comet Wild 2 coma dust particle densities. *Meteoritics & Planetary Science*. 45:1302-1319.

Ikeda S., Nakano T. and Nakashima Y. 2000. Three-dimensional study on the interconnection and shape of crystals in a graphic granite by X-ray CT and image analysis. *Mineralogical Magazine* 64:945–959.

Hutchison R. 2004. *Meteorites: A Petrologic, Chemical and Isotopic Synthesis*. 506 pp. Cambridge Univ. Press, Cambridge.

Macke R. J. (2010) Survey of meteorite physical properties: density, porosity and magnetic susceptibility. Ph.D. thesis, University of Central Florida, 310 pp.

Matsumoto T., Tsuchiyama A., Gucsik A., Noguchi R., Matsuno J., Nagano T., Imai Y., Shimada A., Uesugi M., Uesugi K., Nakano T., Takeuchi A., Suzuki Y., Nakamura T., Noguchi T., Mukai T., Abe M., Yada T. and Fujimura A. 2012. Microstructures of particle surfaces of Itokawa regolith and LL chondrite fragments. *43rd Lunar and Planetary Science Conference* #1969

Michikami T., Nakamura A. M., Hirata N., Gaskell R. W., Nakamura R., Honda T., Honda C., Hiraoka K., Saito J., Demura H., Ishiguro M. and Miyamoto H. 2008. Size-frequency statistics of boulders on global surface of Asteroid 25143 Itokawa. *Earth Planets Space*. 60:13-20.

Miyamoto H., Yano H., Scheeres D. J., Abe S, Barnouin-Jha O., Cheng A. F., Demura H., Gaskell R. W., Hirata N., Ishiguro M., Michikami T., Nakamura A. M., Nakamura R., Saito J. and Sasaki S. 2007. Regolith Migration and Sorting on Asteroid Itokawa. *Science* **316**, 1011-1014.

Nagano T., Tsuchiyama A., Shimobayashi N., Seto Y., Imai Y., Noguchi R., Matsumoto T. and Matsuno J. 2012. Homogeneity of LL5 and LL6 Chondrites in Relation to Hayabusa Sample Analysis. Abstract in *43rd Lunar and Planetary Science Conference* #2500.

Nagao K., Okazaki R., Nakamura T., Miura Y. N., Osawa T., Bajo K., Matsuda S., Ebihara M., Ireland T. R., Kitajima F., Naraoka H., Noguchi T., Tsuchiyama A., Yurimoto H., Zolensky M. E., Uesugi M., Shirai K., Abe M., Yada T., Ishibashi Y., Fujimura A., Mukai T., Ueno M, Okada T., Yoshikawa M. and Kawaguchi J. 2011. Irradiation history of Itokawa regolith material deduced from noble gases in the Hayabusa samples. *Science* 333:1128-1131.

Nakamura E., Makishima A., Moriguti T., Kobayashi K., Tanaka R., Kunihiro T., Tsujimori T., Sakaguchi C., Kitagawa H., Ota T., Yachi Y., Yada T, Abe M., Fujimura A., Ueno M., Mukai T., Yoshikawa M. and Kawaguchi J. 2012. Space environment of an asteroid preserved on micrograins returned by the Hayabusa spacecraft. *Proc. Nat. Acad. Sci*. 109:E624-E629.

Nakamura T., Noguchi T., Tsuchiyama A., Ushikubo T., Kita N. T., Valley J. W., Zolensky M. E., Kakazu Y., Sakamoto K., Mashio E., Uesugi K. and Nakano T. 2008a. Chondrule-like Objects in Short-Period Comet 81P/Wild 2. *Science* 321:1664-1667.

Nakamura T., Tsuchiyama A., Akaki T., Uesugi K., Nakano T., Takeuchi A., Suzuki Y. and Noguchi T. 2008b. Bulk mineralogy and three-dimensional structures of individual Stardust particles deduced from synchrotron X-ray diffraction and microtomography analysis. *Meteoritics & Planetary Science* 43:247-259.

Nakamura T., Noguchi T., Tanaka M., Zolensky M. E., Kimura M., Tsuchiyama A., Nakato A., Ogami T., Ishida H., Uesugi M., Yada T., Shirai S., Fujimura A.,

Okazaki R., Sandford S. A., Ishibashi Y., Abe M., Okada T., Ueno M., Mukai T., Yoshikawa M. and Kawaguchi J. 2011. Itokawa dust particles: A direct link between S-type asteroids and ordinary chondrites. *Science*. 333:1113-1116.

Nakamura T., Nakato A., Ishida H., Noguchi T., Zolensky M. Z., Tanaka M., Kimura M., Tsuchiyama A., Ogami T., Hashimoto T., Konno K., Uesugi M., Yada T., Shirai K., Fujimura A., Okazaki R., Sandford S. A., Ishibashi Y., Abe M., Okada T., Kawaguchi J. 2013. Mineral chemistry of MUSES-C Regio inferred from analysis of dust particles collected from the first and second touchdown sites on asteroid Itokawa. Submitted to *Meteoritics & Planetary Science*.

Nakano T., Nakashima Y., Nakamura K. and Ikeda S. 2000. Observation and analysis of internal structure of rock using X-ray CT. *J. Geol. Soc. Jp.* 106:363-378.

Nakano T., Tsuchiyama A., Uesugi K., Uesugi M. and Shinohara K. 2006. "Slice" -Softwares for basic 3-D analysis- (web). http://www-bl20.spring8.or.jp/slice/, Japan Synchrotron Radiation Research Institute.

Naraoka H., Mita H., Hamase K., Mita M., Yabuta H., Saito K., Fukushima K., Kitajima F., Sandford S. A., Nakamura T., Noguchi T., Okazaki R., Nagao K., Ebihara M., Yurimoto H., Tsuchiyama A., Abe M., Shirai K., Ueno M., Yada T., Ishibashi Y., Okada T., Fujimura A., Mukai T., Yoshikawa M., Kawaguchi J. 2012. Preliminary organic compound analysis of microparticles returned from Asteroid 25143 Itokawa by the Hayabusa mission. *Geochemical Journal*, 46:61-72.

Nelson V. E. and Rubin A. E. 2002. Size-frequency distributions of chondrules and chondrule fragments in LL3 chondrites: Implications for parent-body fragmentation of chondrules. *Meteoritics & Planetary Science* 37: 1361-1376.

Noguchi T., Nakamura T., Kimura M., Zolensky M. E., Tanaka M., Hashimoto T., Konno M., Nakato A., Ogami T., Fujimura A., Abe M., Yada T., Mukai T., Ueno M., Okada T., Shirai K., Ishibashi Y. and Okazaki R. 2011. Incipient space weathering observed on the surface of Itokawa dust particles. *Science* 333:1121-1125.

Noguchi T., Kimura M., Hashimoto T., Konno M., Nakamura T., Zolensky M. E., Tanaka M., Okazaki, R., Tsuchiyama A., Nakato A., Ogami T., Ishida H., Sagae R., Tsujimoto S., Matsumoto T., Matsuno J., Fujimura A., Abe M., Yada T., Mukai T., Ueno M., Okada T., Shirai K., Ishibashi Y. 2013. Space weathered rims found on the 1 surfaces of the Itokawa dust particles. *Meteoritics & Planetary Science* in print.

Rietmeijer F. J. M., Nakamura T., Tsuchiyama A., Uesugi K., Nakano T. and Leroux H. 2008. Origin and formation of iron silicide phases in the aerogel of the Stardust mission. *Meteoritics and Planetary Science* 43:121-134.

Saito J., Miyamoto H., Nakamura R., Ishiguro M., Michikami T., Nakamura A. M., Demura H., Sasaki S., Hirata N., Honda C., Yamamoto A., Yokota Y., Fuse T., Yoshida F., Tholen D. J., Gaskell R. W., Hashimoto T., Kubota T., Higuchi Y.,

Nakamura T., Smith P., Hiraoka K., Honda T., Kobayashi S., Furuya M., Matsumoto N., Nemoto E., Yukishita A., Kitazato K., Dermawan B., Sogame A., Terazono J., Shinohara C. and Akiyama H. 2006. Detailed Images of Asteroid 25143 Itokawa from Hayabusa. *Science*. 312:1341-1344.

Takeuchi A., Uesugi K. and Suzuki Y. 2009. Zernike phase-contrast x-ray microscope with pseudo-Kohler illumination generated by sectored (polygon) condenser plate, *J. Phys.: Conf. Ser.* 186:012020.

Tsuchiyama A., Uesugi K., Nakano T. and Ikeda S. 2005. Quantitative evaluation of attenuation contrast of X-ray computed tomography images using monochromatized beams. *Am. Min.*, 90:132-142.

Tsuchiyama A., Nakamura T., Okazaki T., Uesugi K., Nakano T., Sakamoto K., Akaki T., Iida Y., Kadono T., Jogo K. and Suzuki Y. 2009. Three-dimensional structures and elemental distributions of Stardust impact tracks using synchrotron microtomography and X-ray fluorescence analysis. *Meteoritics & Planetary Science* **44**, 1203-1224.

Tsuchiyama A., Uesugi M., Matsushima T., Michikami T., Kadono T., Nakamura T., Uesugi K., Nakano T., Sandford S. A., Noguchi R., Matsumoto T., Matsuno J., Nagano T., Imai Y., Takeuchi A., Suzuki Y., Ogami T., Katagiri J., Ebihara M., Ireland T. R., Kitajima F., Nagao K., Naraoka H., Noguchi T., Okazaki R., Yurimoto H., Zolensky M. E., Mukai T., Abe M., Yada T., Fujimura A., Yoshikawa M. and Kawaguchi J. 2011. Three-dimensional structure of Hayabusa samples: Origin and evolution of Itokawa regolith. Science. 333:1121-1125.

Tsuchiyama A., Uesugi M., Uesugi K., Nakano T., Noguchi R., Matsumoto T., Matsuno J., Nagano T., Imai Y., Shimada A., Takeuchi A., Suzuki Y., Nakamura T., Noguchi T, Abe M., Yada T., Fujimura A. 2012. Three-dimensional microstructure of particles recovered from asteroid 25143 Itokawa: comparison with LL5 and LL6 chondrite fragments. *Geochimica et Cosmochimica Acta*. http://dx.doi.org/10.1016/j.gca.2012.11.036.

Uesugi K., Takeuchi A. and Suzuki Y. 2006. Development of micro-tomography system with Fresnel zone plate optics at SPring-8. *Proc. SPIE*, 6318:6318F.

Yano H. Kubota T., Miyamoto H., Okada T., Scheeres D., Takagi Y., Yoshida K., Abe M., Abe S., Barnouin-Jha O., Fujiwara A., Hasegawa S., Hashimoto T., Ishiguro M., Kato M., Kawaguchi J., Mukai T., Saito J., Sasaki S., Yoshikawa M. 2006. Touchdown of the Hayabusa spacecraft at the Muses Sea on Itokawa. *Science* 312:1350-1353.

Yurimoto H., Abe K., Abe M., Ebihara M., Fujimura A., Hashiguchi M., Hashizume K., Ireland T. R., Itoh S., Katayama J., Kato C., Kawaguchi J., Kawasaki N., Kitajima F., Kobayashi S., Meike T., Mukai T., Nagao K., Nakamura T., Naraoka H., Noguchi T., Okazaki R., Park C., Sakamoto N., Seto Y., Takei M., Tsuchiyama A., Uesugi M., Wakaki S., Yada T., Yamamoto K., Yoshikawa M. and Zolensky M. E.

2011. Oxygen isotopic compositions of asteroidal materials returned from Itokawa by the Hayabusa mission. *Science* 333:1116-1119.

Figure captions

Figure 1. Cumulative size distribution of the Itokawa particles collected from quartz plates (tapping samples). The sphere-equivalent diameters of 47 particles by tomography and the apparent largest diameters of 164 particles by SEM are shown.

Figure 2. Three-dimensional shape distributions of Itokawa particles. Fragments of impact experiments (Capaccioni et al., 1984) are also shown. Large circles shows particles with rounded edges.

Figure 3. Slice images of Itokawa particles obtained from microtomography with a gray scale showing the linear attenuation coefficient (LAC) of objects (from 0 to X cm^{-1}), where X is the maximum LAC value in the CT images. (A) Itokawa particle RA-QD02-0023 (8 keV, X = 575 cm^{-1}). (B) Ensisheim meteorite (E4-10) (7 keV, X = 431 cm^{-1}). (C) Itokawa particle RA-QD02-0030 (7 keV, X = 719 cm^{-1}). (D) Ensisheim meteorite (E2-6) (7 keV, X = 431 cm^{-1}). (E) Itokawa particle RA-QD02-0013 (7 keV, X = 575 cm−1). (F) Tuxtuac meteorite (T-12) (7 keV, X = 719 cm^{-1}). (G) Itokawa particle RA-QD02-0019 (7 keV, X = 287 cm^{-1}). (H) Tuxtuac meteorite (T-15) (8 keV, X = 1437 cm^{-1}). (I) Itokawa particle RA-QD02-0062-1 (7 keV, X = 287 cm^{-1}). (H) Kilabo meteorite (E3-09) (7 keV, X = 719 cm^{-1}). The concentric structure is a ring artifact. The bright edges of the particles and voids are artifacts resulting from refraction contrast. Ol: olivine; LPx: low-Ca pyroxene; HPx: high-Ca pyroxene; Pl: plagioclase; and Tr: troilite.

Figure 4. Bird's eye view images showing the distribution of voids in the Itokawa particle RA-QD02-0014. (A) Top view. (B) Side view. (C) Side view rotated from (B) by 90 deg. Small void inclusions define a 3D plane (A and B). Most of the small voids, which are platy and have facets, are located along the 3D plane with common directions of their longest axes (C). Voids with tube shapes (arrows), which are not located on the plane, are also seen. The size of the box is 63 μm × 63 μm × 122 μm.

Figure 5. Histograms for porosity. (A) Itokawa particles. (B) LL5 and LL6 chondrite particles.

Table 1. A list and summary of Itokawa particles.

sample ID	volume	sphere-equivalent diameter	longest axis length, a	medium axis length, b	shortest axis length, c	porosity	mode (vol.%)*								porous#	small void inclusions#	void tubes#	cracks#	edges$	remarks
	μm³	μm	μm	μm	μm	%	Ol	LPx	HPx	Pl	Tr	Tae	Kam	Chm	Ca-P					
RA-QD02-0009	26282	36.9	80.2	53.3	18.9	8.8	12.8	81.6		5.6							C	C		A	
RA-QD02-0010	480841	97.2	148.9	124.9	59.8	0.0	67.1	5.1	3.8	23.1	0.7	0.1	0.1							A	
RA-QD02-0011-1	11433	28.0	47.4	36.5	25.6	11.0	40.5		39.6	20.0							C			A	
RA-QD02-0011-2	83948	54.3	80.1	60.8	36.8	0.3	91.9		2.8	4.3	0.8	0.2					P			R	
RA-QD02-0013	236244	76.7	91.0	79.9	70.8	4.8	61.8	3.1	4.7	30.0		0.4				C	C	C		R	
RA-QD02-0014	125921	62.2	131.3	57.3	38.1	0.7	92.4	6.9		0.7							P			A	
RA-QD02-0016	18445	32.8	58.0	43.8	17.5	0.2	85.0	9.4	3.6	1.3	0.6	0.2					R			A	
RA-QD02-0017	16305	31.5	45.0	34.8	22.6	0.0	92.8		7.2											A	
RA-QD02-0019	76706	52.7	98.3	53.9	31.6	3.9	93.3			4.8	2.0						C	C		A	
RA-QD02-0021	11563	28.1	56.5	33.7	17.0	6.5		95.1	4.5		0.4						R		C	A	
RA-QD02-0023	781081	114.3	149.5	119.6	98.0	0.0	99.6				0.4									A	
RA-QD02-0024	154338	66.6	90.0	77.4	48.5	1.9	50.5	17.1	22.6	9.6	0.2	0.0					R			A	
RA-QD02-0025-01	10348	27.0	51.9	28.4	16.3	2.6			0.3	99.7							C	C		A	
RA-QD02-0025-02	2392	16.6	28.3	22.8	8.9	0.0				100.0										A	
RA-QD02-0027	88478	55.3	83.0	56.0	41.5	3.5		11.0		18.4	70.6						P		C	A	
RA-QD02-0028	18353	32.7	55.3	37.4	20.4	0.0	97.0	2.6			0.3	0.1					R			A	
RA-QD02-0030	760742	113.3	163.8	149.9	70.0	0.0	31.7	51.4	0.8	14.6	0.5	1.0								R	
RA-QD02-0031	317089	84.6	166.7	98.1	42.9	0.0	79.3		1.7	14.1	3.4			1.5						A	
RA-QD02-0032	12988	29.2	41.3	30.8	21.5	7.4	58.6	0.6	30.8	10.1							C			R	
RA-QD02-0033	61505	49.0	63.3	53.7	42.2	7.6	82.0	0.2	8.2	8.1	0.0			0.0	1.5	C	C			R	
RA-QD02-0034	9304	26.1	53.6	25.2	18.1	8.0	56.3	29.8	11.4		2.5								C	A	
RA-QD02-0036	7905	24.7	47.4	31.9	14.3	0.1	77.1			22.9										A	
RA-QD02-0038	19486	33.4	54.7	43.0	19.1	4.4	9.4	81.7		3.7	5.1			0.1			R			A	
RA-QD02-0039	15331	30.8	54.6	33.8	19.3	5.2	70.4	14.3	9.2	5.1	1.0						C	C		A	
RA-QD02-0041	117363	60.7	88.6	63.2	47.4	2.8	90.8		0.3	8.9							C			A	
RA-QD02-0042	211529	73.9	96.1	78.4	61.3	0.0	3.3	90.9	1.1	4.4	0.3	0.0	0.0				R			R	
RA-QD02-0043	172425	69.1	87.4	72.9	59.4	4.6	92.6		3.7	3.6	0.1						C	C		A	
RA-QD02-0047	148570	65.7	107.9	92.1	32.2	0.0	95.3	2.8	1.9											A	
RA-QD02-0048	29360	38.3	57.5	43.7	27.4	6.0	74.8	1.1	10.8	13.2	0.1					C	C	C		R	
RA-QD02-0049-2	8308	25.1	55.9	20.6	17.9	0.9	92.1		0.4	7.0	0.6						P			A	broken piece
RA-QD02-0050	26287	36.9	80.3	30.1	28.5	5.3	71.7		17.4	10.9									C	R	
RA-QD02-0054	8032	24.8	36.6	25.3	20.4	0.0	99.6				0.4									A	
RA-QD02-0055	17906	32.5	56.1	33.3	21.2	2.9			1.7	98.1	0.2									A	
RA-QD02-0057	24527	36.0	60.7	35.9	27.2	2.0		100.0												A	
RA-QD02-0058	25839	36.7	53.4	39.1	27.6	7.2	76.1	4.0	4.8	15.1						C	C	C		R	
RA-QD02-0060	19912	33.6	59.2	34.0	26.8	9.9	39.1	48.6	3.5	8.8						C	C	C		R	
RA-QD02-0061	33111	39.8	49.3	39.2	36.9	1.5	7.9	87.4		4.2	0.5	0.1								A	
RA-QD02-0062-1	6780	23.5	35.6	30.2	15.6	9.3	73.2	26.8									C		C	A	
RA-QD02-0062-2	1295	13.5	20.5	13.8	10.0	0.0														A	
RA-QD02-0063	36507	41.2	58.2	46.3	34.1	6.3	35.4	52.4	5.0	5.7	0.1				1.3		P		C	R	
RA-QD02-0064	13427	29.5	55.4	32.4	18.7	2.2	100.0										C	C		R	
RA-QD02-0066	18477	32.8	64.7	52.8	14.0	5.3	100.0												C	A	
RA-QD02-0067	9497	26.3	46.9	40.1	11.5	0.0	52.6			47.4										A	
RA-QD02-0068	54978	47.2	98.5	52.6	32.3	7.2	63.3	0.7	2.2	31.3	2.2	0.3					C	C		A	
RB-QD04-0006	6247	22.8	26.6	25.2	21.1	4.9	84.4	4.6		9.2	1.8						C	C		R	
RB-QD04-0023	8474	25.3	50.0	33.6	12.3	3.4	88.6		11.4								C	C		A	
RB-QD04-0025	7277	24.0	36.0	29.2	18.5	0.0	8.5	75.2		3.3					13.1					A	
RB-QD04-0049	14402	30.2	45.9	32.1	26.4	3.2	83.8		6.4	7.9	0.0						C	C		A	

* Ol: olivine, LPx: low-Ca pyroxene, HPx: high-Ca pyroxene, Pl: plagioclase, Tr: troilite, Tae: taenite, Kam: kamacite, Chm: chromite, Ca-P: Ca phosphates

"0.0 vol/%" means that the mineral is present but its mode is <0.05 vol.%. Blank means "not determined" even if a very small amount of the mineral is present.
[#] C: common, P: present, R: rare
[$] A: angular, R: rounded

Table 2 Samples and their size parameters.

sample	Number of particles	Total volume (μm^3)	Sphere equivalent diameter (μm)	Median diameter (μm)
Itokawa				
All	48	4367554	202.8	33.5
Room-A	44	4331154	202.2	36.4
Room-B	4	36400	41.1	24.7
Previous data*	40	4231738	200.7	36.8
LL5,6 chondrites				
All	40	4820240	209.6	47.5
LL6	25	4324360	202.1	58.5
Ensisheim	15	1878198	153.1	52.2
Kilabo	10	2446162	167.2	62.3
LL5 (Tuxtuac)	15	495880	98.2	38.6

* Room-A particles (Tsuchiyama et al., 2011)

Table 3 Modal abundances of minerals of Itokawa and LL5,6 chondrite particles and ordinary chondrites.

vol.%	olivine	low-Ca pyroxene	high-Ca pyroxene	plagioclase	troilite	kamacite	taenite	chromite	Ca-phosphates	Porosity
Itokawa samples										
All	64.94	18.61	2.82	11.16	2.07	0.22	0.01	0.11	0.06	1.45
Room-A	64.90	18.64	2.80	11.21	2.08	0.22	0.01	0.11	0.03	1.44
Room-B	69.88	15.88	5.16	5.34	0.33	0.00	0.00	0.00	3.40	2.90
Previous data*	64.44	19.02	2.72	11.34	2.12	0.22	0.02	0.11	0.01	1.35
LL chondrite samples										
All	63.88	7.92	8.69	14.51	3.68	0.37	0.00	0.93	0.00	1.91
LL6	65.89	7.29	9.19	15.00	1.46	0.14	0.00	1.02	0.00	1.66
Ensisheim	61.34	12.89	5.40	17.10	1.30	0.09	0.00	1.88	0.00	1.69
Kilabo	69.39	2.99	12.11	13.38	1.59	0.18	0.00	0.36	0.00	1.64
LL5 (Tuxtuac)	46.32	13.42	4.32	10.29	23.10	2.40	0.00	0.15	0.00	4.11
Ordinary chondrites**										
H4-6	~38	~28	~6	10	5	10#		<1	<1	
L4-6	~48	~24	~6	10	5	<5#		<1	<1	
LL4-6	~58	~16	~6	10	5	2#		<1	<1	
wt.%										
Itokawa samples (All)	67.17	18.10	2.58	8.50	2.89	0.52	0.03	0.15	0.05	
LL chondrite samples (All)	65.97	7.69	7.94	11.04	5.14	0.90	0.00	1.31	0.00	
Ordinary chondrites***										
H4	29.8(1.4)	27.0(1.9)	7.3(0,2)	9.1(0.1)	6.0(0.7)					
H5	33.1(2.0)	25.2(1.1)	7.2(0.7)	8.9(0.7)	5.9(0.8)					
H6	35.7(2.2)	24.9(2.1)	5.7(0.6)	8.9(0.4)	5.6(0.9)					
L4	40.7(1.9)	23.6(1.8)	8.8(1.3)	9.5(0.4)	7.0(1.8)					
L5	42.2(2.0)	24.2(1.3)	7.7(1.2)	9.3(1.5)	6.8(2.3)					
L6	43.0(1.6)	21.7(0.9)	8.1(0.4)	9.5(0.5)	8.0(1.9)					
LL4	49.7(1.5)	22.6(1.4)	7.6(1.5)	9.7(1.2)	3.8(1.0)					
LL5	51.1(1.1)	21.8(1.4)	7.2(0.7)	9.6(0.6)	3.8(0.9)					

LL6	52.5(3.1)	18.9(1.0)	7.5(0.6)	9.8(0.7)	2.6(1.8)

* Room-A particles (Tsuchiyama et al., 2011)
** Modal abundance in vol.% (Hutchison, 2004)
*** Modal abundance in wt.% (Dunn et al., 2010)
# The modal abundance of metals (kamacite and taenite)

Table 4 Numbers and volume % of particles with various properties.

Samples	Polymineralic		Void-rich		Poroous		Small void inclusion-rich		Void tube present		Crack-rich		Rounded edge present	
	N	vol.%	N	vol.%	N	vol.%	N	vol.%	N	vol.%	N	vol.%	N	vol.%
Itokawa														
All	21	52.9	19	21.1	5	8.5	19	21.1	14	16.3	7	4.5	13	34.9
Room-A	20	53.2	16	20.6	5	8.6	16	20.6	11	15.7	7	4.6	12	35.1
Room-B	1	20.0	3	80.0	0	0.0	3	80.0	3	80.0	0	0.0	1	17.2
LL chondrites														
All	23	51.0	8	6.7	5	3.5	6	5.5	3	2.3	19	47.9	n.d.	n.d.
LL6	13	48.0	0	0.0	0	0.0	0	0.0	0	0.0	8	44.6	n.d.	n.d.
Kilabo	6	46.3	0	0.0	0	0.0	0	0.0	0	0.0	6	66.2	n.d.	n.d.
Ensisheim	7	50.2	0	0.0	0	0.0	0	0.0	0	0.0	2	16.6	n.d.	n.d.
LL5 (Tuxtuac)	10	77.6	8	64.9	5	34.1	6	53.9	3	22.5	11	76.7	n.d.	n.d.

n.d. not determined

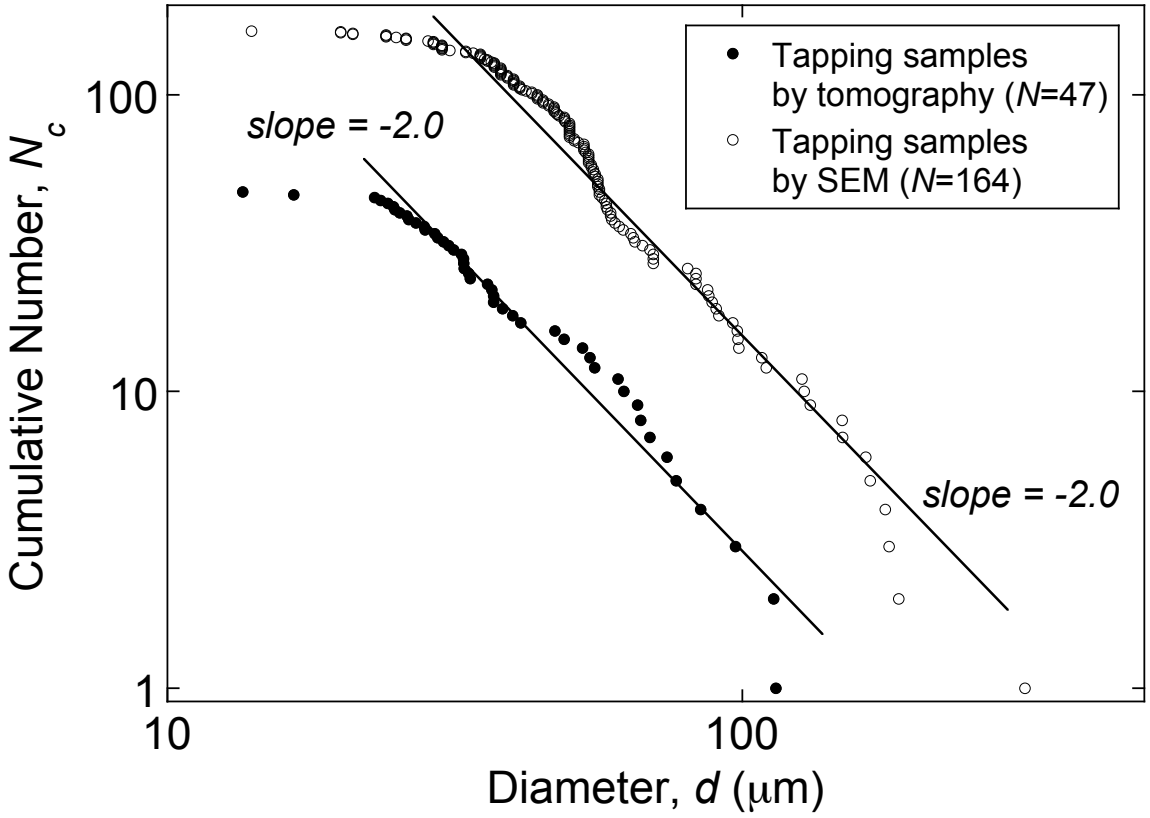

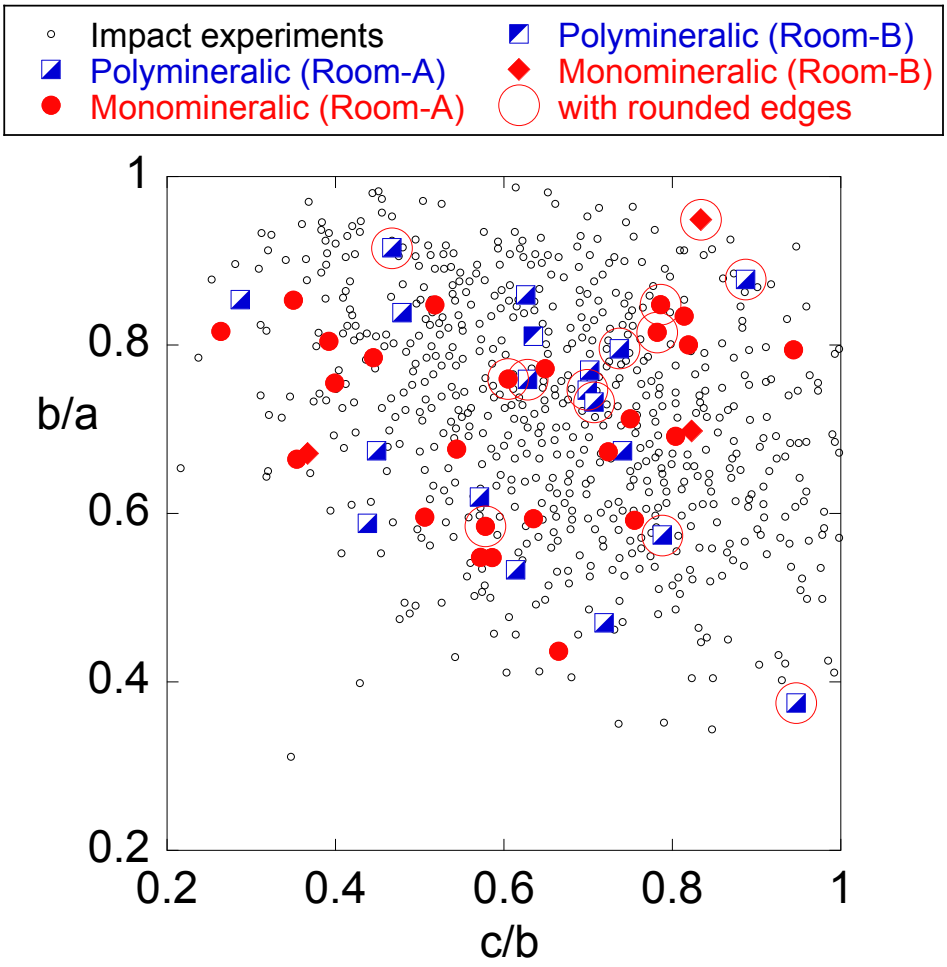

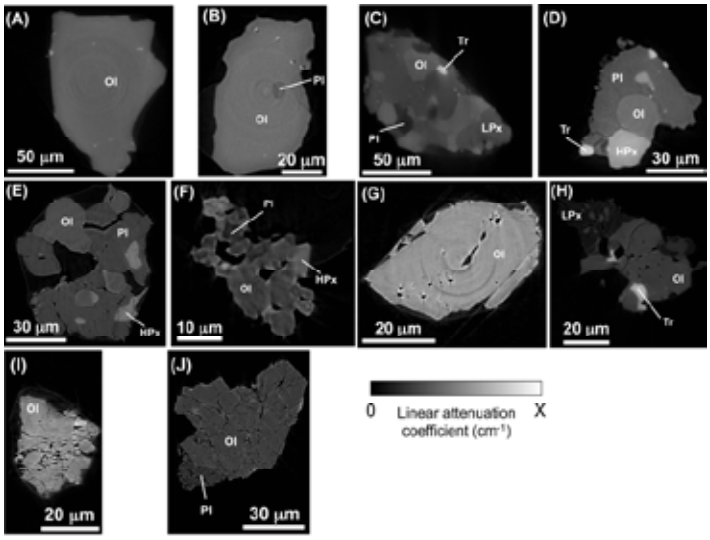

175x132mm (300 x 300 DPI)

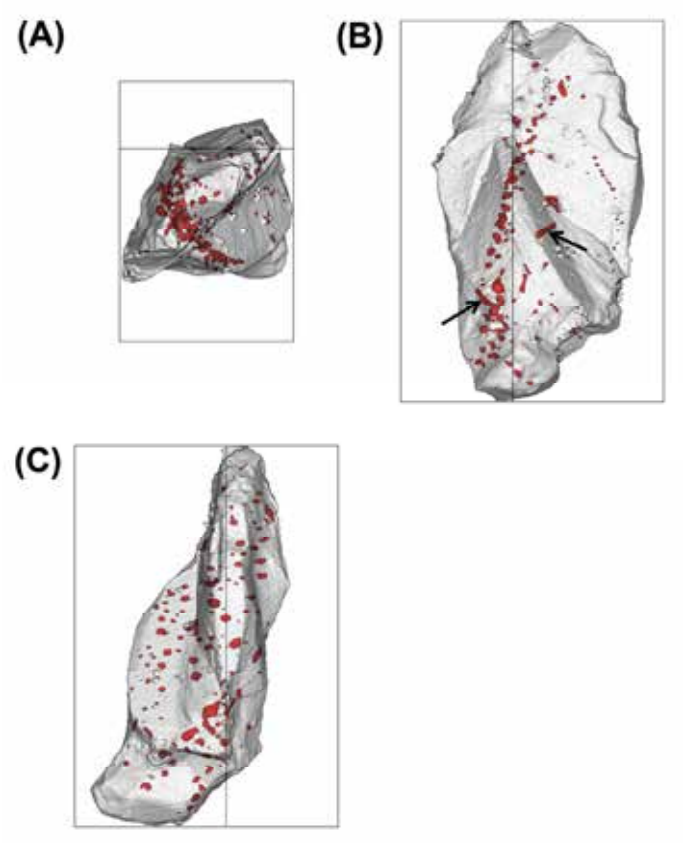

124x154mm (300 x 300 DPI)